



Human body radiation area factors for diverse adult population

Konrad Rykaczewski^{1,2} · Lyle Bartels¹ · Daniel M. Martinez¹ · Shri H. Viswanathan¹

Received: 14 May 2022 / Accepted: 30 August 2022 / Published online: 8 September 2022
© The Author(s) under exclusive licence to International Society of Biometeorology 2022

Abstract

Radiation accounts for a significant fraction of the human body and environment heat exchange and strongly impacts thermal comfort and safety. The direct radiative exchange between an individual and a source or sink can be quantified using the effective (f_{eff}) and projected radiation area factors (f_p). However, these factors have not been quantified for half of the population of the USA with an above-average body mass index (BMI). Here, we address this gap by developing thirty male and thirty female computational manikin models that cover the 1 to 99 percentile variation in height and BMI of adults in the USA. The radiative simulations reveal that the f_{eff} and the f_p angular distributions are nearly independent of gender, height, and BMI. Appreciable relative differences from the average models only emerge for manikins with BMI above 80th percentile. However, these differences only occur at low zenith angles and, in absolute terms, are small as compared to variations induced by, for example, the zenith angle increase. We also use the manikin set to evaluate whether the body shape impacts the quality of human representation with several levels of geometrical simplification. We find that the “box/peg” body representation, which is based on the hemispherical f_p average, is independent of the body shape. In turn, the f_p distributions averaged over the azimuth angle range, representing the rotationally symmetric humans, are only impacted to the same degree as for the anatomical manikins. We also show that the anatomical manikins can be closely approximated by the multi-cylinder and sphere representation, at least from a radiation perspective. The developed anatomical manikin set is freely available and can be used to compute how body shape impacts a variety of external heat transport processes.

Keywords Human radiative heat exchange · Effective radiation area factor · Projected area factor · Diverse body shapes · Human radiation geometry

Abbreviations

| | |
|------------|--|
| A_{eff} | Effective radiation area (m ²) |
| A_p | Projected radiation area (m ²) |
| A_t | Total body surface area (m ²) |
| <i>BMI</i> | Body mass index (kg/m ²) |
| f_{eff} | Effective radiation area factor |
| f_p | Projected radiation area factor |
| F_{s-m} | Sphere-manikin view factor |
| θ | Zenith angle (°) |

Introduction

Radiation accounts for a significant fraction of human body and environment heat exchange and often plays a defining role in an individual’s thermal comfort and safety levels. These characteristics degrade when radiation exposure is anisotropic (Parsons 2014). In indoor settings, being next to a cold window or infrared heater can cause thermal discomfort and proximity to a hot manufacturing process, such as metal casting, can be very dangerous (Kubaha et al. 2004). In outdoor settings, even with extremely hot air temperatures, direct solar radiation can cause substantially more heating of the human body than air convection (Parsons 2014; Ioannou et al. 2021). Naturally, the amount of direct radiative heating depends on the relative orientation between the individual and the radiation source as well as body size and posture (Fanger 1972).

The direct radiative heat exchange between an individual and a source or sink is often quantified in terms of the total body area (A_t), the body surface exposed to surrounding radiant

Lyle Bartels, Daniel M. Martinez, and Shri H. Viswanathan contributed equally to this work.

✉ Konrad Rykaczewski
konradr@asu.edu

¹ School for Engineering of Matter, Transport and Energy, Arizona State University, Tempe, AZ 85287, USA

² Julie Ann Wrigley Global Futures Laboratory, Arizona State University, Tempe, AZ 85287, USA

environments (i.e., the effective radiation area A_{eff}), and the body surface exposed to the direct radiation (i.e., the projected area A_p). For generalization, these areas are combined into the effective radiation area factor ($f_{eff} = A_{eff}/A_t$) and the projected radiation area factor ($f_p = A_p/A_{eff}$). While these two factors have been quantified by numerous studies in the last 90 years, primarily young “average” individuals have been measured (Bandow and Bohnenkamp 1935; Guibert and Taylor 1952; Underwood and Ward 1966; Fanger 1972; Steinman et al. 1988; Horikoshi 1990; Rizzo et al. 1991; Blazejczyk et al. 1993; Jones et al. 1998; Park and Tuller 2011a) or simulated (Tanabe et al. 2000; Kubaha et al. 2003, 2004; Rees et al. 2008; Yousaf et al. 2008; Rykaczewski et al. 2022). Similarly, radiation heat transfer coefficients, which can be converted into the two radiation area factors (Wissler 2018), have been quantified using near “average” human subjects or corresponding thermal manikins (Winslow et al. 1940; Mitchell et al. 1969; de Dear et al. 1997; Manabe et al. 2004; Quintela et al. 2004). Furthermore, as Park and Tuller (2011a) pointed out, the few prior studies that investigated how the two radiation area factors are impacted by body shape relied on small subject numbers and limited measurements (Bandow and Bohnenkamp 1935; Guibert and Taylor 1952; Underwood and Ward 1966; Horikoshi 1990). The two authors addressed this knowledge gap for normal weight and overweight subjects (Park and Tuller 2011a) and only found minor impact of body shape on the two radiation area factors.

Unfortunately, due to the continuing “trend towards more overweight people” that motivated Park and Tuller’s study and country-to-country population differences, their results do not cover half of the adult population of the USA today. In particular, the mean body mass index ($BMI = \text{weight [kg]} / \text{height [m]}^2$) for the over-weight subjects in their study was about 27 (Park and Tuller 2011a), which is about equal to the average BMI of adults in the USA (Center for Disease Control and Prevention 2022). Furthermore, 40% and 9% of adults in the USA have BMI over 30 (obese) and over 40 (severely obese), respectively (Center for Disease Control and Prevention 2022). Upon even a simple visual inspection of adult male manikins representing 1% to 99% BMI variation in the USA shown in Fig. 1, Park and Tuller’s results are not surprising. In particular, the geometrical differences between the manikins with BMI of 23 (the mean normal weight for Park and Tuller study) and 27 are minor. In contrast, major geometrical differences emerge as the BMI increases above 75% ($\sim 32 \text{ kgm}^{-2}$), which indicates that the body shape might impact radiation area factors. We also highlight that obesity rates are the highest among American African and Hispanic adults (Center for Disease Control and Prevention 2022) and that communities of color in most large cities in the USA are disproportionately impacted by heat (Hsu et al. 2021). In other words, we are missing important knowledge about radiative exposure of the population segment that is at increased risk of extreme heat exposure.

In this work, we begin to address this gap by computing the effective and projected radiation area factors for thirty male and thirty female computational manikin models that cover 1 to 99% variation in height and BMI of adults in the USA. We also use the developed computational manikin set to evaluate whether the body shape impacts the quality of human representation with several levels of geometrical simplification.

Methods

Computational manikin generation

We used the Open Design Lab Manikin Fetcher tool based on the US National Health and Nutrition Examination Survey (NHANES) to generate the three-dimensional male and female manikins that represent 1 to 99% height and BMI diversity of the adult US population (Parkinsons n.d.). In particular, we generated twenty-five manikins for each gender, covering each height and BMI percentile combination in about 25% increments (see Fig. 1), and additional five with 50% height and high range BMI. The Manikin Fetcher tool generates manikins near the requested height and BMI combination. For example, for the requested female manikin with 50% BMI and 50% height, a model with 49.3% BMI (27.1 kgm^{-2}) and 50.4% height (162.1 cm) might be generated. To facilitate the presentation of the results, we refer to the manikins by the approximate percentile values, while the exact anthropometric data for each of them are included in parenthesis and also are tabulated in the Supplementary Information.

To generate “watertight” quality meshes for the finite element method (FEM) radiation simulations, we exported the file from the manikin fetcher tool in *.jt* format, then converted to *.ply* format to be used in the 3D mesh processing software system, MeshLab. In MeshLab, we cleaned the imported mesh of all non-manifold edges and vertices as well as duplicate faces and vertices. Subsequently, we imported the manikin into InstantMesh software and used it to refine the mesh to have uniform topology with increased vertex density. After using InstantMesh, we re-imported the mesh as a *.ply* file into MeshLab where we removed the scalp hair along with any other unwated deformities. Next, we conducted a Poisson reconstruction of the model with a minimum sample size of 15 and the pre-clean option selected. While this step creates a watertight “shell” of the model, some defects can arise around the hands, armpits, and groin areas. We addressed these defects manually in MeshLab or after importing the *.stl* format meshes into Comsol Multiphysics 6.0. In the latter software, we followed our prior procedure (Rykaczewski et al. 2022) to eliminate any defects and re-mesh the geometries with sufficient element density

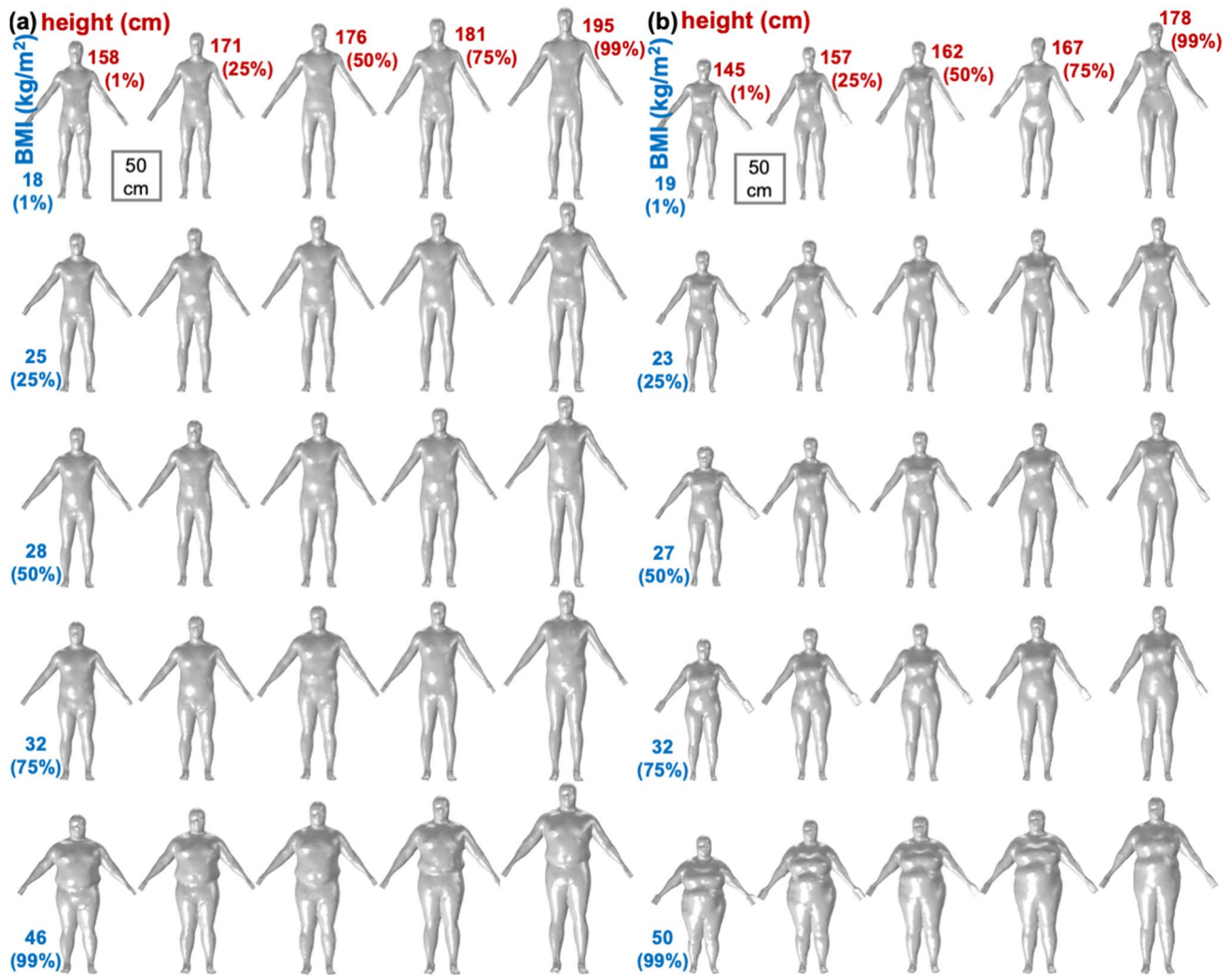


Fig. 1 The processed and finalized twenty-five anatomically representative **a** male and **b** female computational manikins employed in the simulations

for the FEM simulations (i.e., “finer” size, see mesh refinement study in our prior work (Rykczewski et al. 2022)).

All the manikin models generated by the Manikin Fetcher tool include summer clothing (shorts and T-shirt), have scalp hair, have resolved fingers, and are in a standing pose with arms raised at 35° away from the trunk. As in our prior work (Rykczewski et al. 2022), the final meshes used in radiation simulations include the clothing, which increases the effective radiation area. As a result, the f_{eff} that we compute corresponds to the product of the effective radiation area of nude subjects (as f_{eff} was defined by Fanger (1972)) with the clothing area factor, f_{cl} . For the near “average” young adults that participated in his radiation-oriented experiments and were wearing long sleeve shirts and pants, Fanger measured an average f_{cl} of 1.19. This value likely decreases only mildly for the summer clothing, to a range of 1.12 to 1.15 (Smallcombe et al. 2021). Our simulated values of this

“combined” f_{eff} of 0.85 for the average male subject with arms along the trunk matched well with Fanger’s 0.86 ± 0.03 (0.725×1.19) value and Park and Tuller’s $f_{eff} = 0.84$ value for adults wearing swimsuits (Rykczewski et al. 2022). We deem this an appropriate approach since adults wear summer clothing in hot weather in most situations of interest. In addition, the change in these results would be small since f_{cl} increases only mildly between short and full-length clothing. However, in the case of scalp hair, we decided that removing it from the final manikin meshes will provide the most general results. In particular, the variation of scalp hair has been recently shown to strongly impact solar radiation received by the head (Lasisi et al. 2020). Thus, the radiation area factors simulated for our “hair-less” manikins can be augmented if the impact of specific scalp hair geometry is known. In turn, we edited the geometry of the hands for more pragmatic reasons.

The regions around the fingers have the most complex topology, leading to multiple mesh defects such as self-intersecting elements. The proximity of the fingers can also result in the formation of artifacts such as partial merging or shortening of fingers during the mesh processing process. To systematically avoid such issues, we replaced the distal section of the hand that includes fingers with an extrusion of the cross-section of the cut. We adjusted the extrusion length to preserve the effective radiation area of the removed hand section. We evaluated “peg-like” hands made from extrusion of the cross-section made at the wrist and a “mitten-finger” hand made from a cut around the metacarpophalangeal thumb joint. Since the perimeter of the cut made about the metacarpophalangeal thumb joint (~25 cm) is much larger than that made around the wrists (~15 cm), the length of the “mitten-finger” extrusion is significantly shorter. Although, as we describe in detail in the Supplementary Information the two approaches yield essentially identical results from a radiative perspective, we selected to proceed with the “mitten-finger” route because it provides more human-like geometry. Lastly, we selected to keep the pose the same for all the manikins. As also found by Yousaf et al. (2008), raising the arms away from the trunk increases the value of f_{eff} (e.g., from 0.85 to 0.91 for average male manikin (Rykaczewski et al. 2022)). Figure 1 shows the frontal view of all the finalized fifty manikins, including the approximate BMI and height values and percentiles.

Formulation of the effective radiation area and projected radiation area factor simulation

To compute the A_t , A_{eff} , and A_p values, we employ the computational framework developed and validated in our recent work (Rykaczewski et al. 2022). To reiterate briefly, we conduct all simulations using the Surface-to-Surface Radiation node in the Heat Transfer module of Comsol Multiphysics 6.0. The effective radiation area is computed from simulated view factor (F_{s-m}) between a large sphere with an area A_s and centrally placed manikin as $A_{eff} = A_s F_{s-m}$ (Fanger 1972; Yousaf et al. 2008). The projected radiation area is computed from a simulation of irradiation on a planar wall placed behind the manikin exposed to a 500 Wm^{-2} “External Radiation Source” with an “Infinite distance” position and direction corresponding to the angular orientation of interest. We employed the Hemicube method with 64 resolution that yielded the same results as the default 256 resolution. For each manikin, we simulated the zenith angle range of $0 \leq \theta \leq 90^\circ$ and azimuth angle range of $0 \leq \alpha \leq 360^\circ$ (see Fig. S1 in the Supplemental Information for the angle orientation definitions) with recommended 10° increments (Park and Tuller 2011a). As we describe in the Supplemental Information, by simulating the entire azimuth range and averaging the results for the two manikin sides, we negate

any minor artifacts stemming from the slight asymmetry of the manikin leg pose (Rykaczewski et al. 2022). We simulated over 17,000 effective and projected area cases using the ASU High Performance Computing Agave cluster.

Results

Total and effective radiation areas, and effective radiation area factor

The total and effective radiation areas increase with both BMI and height of the manikins (see Table 1). The A_t of most manikins is within 10% of the value calculated by the DuBois formula (Dreyfuss and Dreyfuss 1967), with a variation of at most 20% occurring for a few of the tallest manikins (see Tables S1 and S2 in the Supplemental Information). While a significant fraction of these differences in the total surface area of the manikin and the DuBois area likely stems from the clothing factor, even the largest variation is within expected uncertainty for the DuBois formula (Redlarski et al. 2016). The effective radiation areas scale remarkably closely with the total surface area. In particular, the f_{eff} is 0.92 for all the male manikins and within 0.90 to 0.92 for the female manikins. These values are consistent with prior results (Yousaf et al. 2008; Rykaczewski et al. 2022) and indicate that most of the surface body area of clothed adults with arms raised away from the trunk participates in radiation exchange with the surrounding.

The projected radiation area factors

Our projected radiation area factor angular distributions for the average size manikins match closely with each other and with prior literature. The plot in Fig. 2a shows that the simulated f_p distributions at the four example θ values for the average male manikin (50% BMI (28 kgm^{-2}) and 50% height (176 cm)) with hands oriented vertically along with the trunk match within 10% those measured by Fanger (1972). These minor discrepancies occur predominantly around α of 45° , 90° , and 135° and likely stem from minor differences in the pose of the simulated manikin and the human subjects in the seminal experiments (who had arms touching the trunk). Similarly, the plot in Fig. 2b shows that, independent of the arm orientation, the f_p values for all the average male (arms along and away from the trunk) and female (arms away from the trunk) manikins match closely. The largest f_p difference between the poses occurs at the zenith angle of 0° . Under this top-down irradiation, raising the manikin arms away from the trunk increases the f_p value from about 0.08 to 0.1. This increase is expected since raising the arms increases the “shadow” casted under the manikins. Next, we

Table 1 The total (A_t) and effective radiation (A_{eff}) areas and effective radiation area factor (f_{eff}) for the fifty anatomical manikins with BMI and height percentiles (%) indicated

| BMI, % | Height, % | Female | | | Male | | |
|--------|-----------|------------------------|----------------------------|-----------|------------------------|----------------------------|-----------|
| | | A_t , m ² | A_{eff} , m ² | f_{eff} | A_t , m ² | A_{eff} , m ² | f_{eff} |
| 1 | 1 | 1.20 | 1.10 | 0.91 | 1.43 | 1.32 | 0.92 |
| 1 | 25 | 1.20 | 1.11 | 0.92 | 1.51 | 1.39 | 0.92 |
| 1 | 50 | 1.27 | 1.16 | 0.91 | 1.58 | 1.46 | 0.92 |
| 1 | 75 | 1.40 | 1.29 | 0.92 | 1.70 | 1.57 | 0.92 |
| 1 | 99 | 1.58 | 1.44 | 0.91 | 1.84 | 1.69 | 0.92 |
| 25 | 1 | 1.26 | 1.14 | 0.91 | 1.52 | 1.40 | 0.92 |
| 25 | 25 | 1.39 | 1.27 | 0.91 | 1.77 | 1.62 | 0.92 |
| 25 | 50 | 1.44 | 1.31 | 0.91 | 1.75 | 1.61 | 0.92 |
| 25 | 75 | 1.55 | 1.40 | 0.90 | 1.82 | 1.67 | 0.92 |
| 25 | 99 | 1.66 | 1.51 | 0.91 | 2.04 | 1.87 | 0.92 |
| 50 | 1 | 1.51 | 1.37 | 0.90 | 1.58 | 1.45 | 0.92 |
| 50 | 25 | 1.50 | 1.36 | 0.91 | 1.79 | 1.64 | 0.92 |
| 50 | 50 | 1.60 | 1.45 | 0.90 | 1.89 | 1.73 | 0.92 |
| 50 | 75 | 1.64 | 1.49 | 0.90 | 1.94 | 1.78 | 0.92 |
| 50 | 99 | 1.79 | 1.61 | 0.90 | 1.99 | 1.83 | 0.92 |
| 75 | 1 | 1.43 | 1.29 | 0.90 | 1.68 | 1.54 | 0.92 |
| 75 | 25 | 1.61 | 1.46 | 0.91 | 1.90 | 1.75 | 0.92 |
| 75 | 50 | 1.75 | 1.58 | 0.90 | 2.02 | 1.85 | 0.92 |
| 75 | 75 | 1.75 | 1.58 | 0.90 | 1.97 | 1.81 | 0.92 |
| 75 | 99 | 1.77 | 1.62 | 0.92 | 2.23 | 2.04 | 0.92 |
| 99 | 1 | 1.74 | 1.62 | 0.93 | 2.06 | 1.89 | 0.92 |
| 99 | 25 | 1.98 | 1.83 | 0.92 | 2.19 | 2.01 | 0.92 |
| 99 | 50 | 2.07 | 1.91 | 0.92 | 2.20 | 2.03 | 0.92 |
| 99 | 75 | 2.18 | 2.01 | 0.92 | 2.36 | 2.16 | 0.92 |
| 99 | 99 | 2.23 | 2.06 | 0.92 | 2.46 | 2.26 | 0.92 |

discuss how changing the body shapes away from the average BMI and height impacts the f_p values.

The projected radiation area factor distributions are nearly independent of the gender and height of the manikins and are only moderately impacted by BMI at its largest values. For example, the plot in Fig. 2c shows that for male manikins with 50% BMI (28 kgm⁻²), varying the height does not impact the f_p distribution. The same trend can be observed in the corresponding plot for female manikins shown in the Supplemental Information. In turn, the plot in Fig. 2d shows that for the male manikins with 50% height (176 cm), only the manikin with 99% BMI (46 kgm⁻²) has a distinguishable f_p distribution (highlighted in black in the plot to facilitate interpretation). Even in this case, the differences become appreciable ($\geq 10\%$) only for lower zenith angle values (e.g., at θ of 30° and α of 90°). The most considerable difference of around 20% occurs for top-down irradiation. The corresponding plot for female manikins with 50% height (162 cm) and varied BMI shown in the Supplemental Information demonstrates the same trend but with the most significant difference from the average of about 30% occurring for the 99% BMI (50 kgm⁻²) manikin.

Indeed, Table 2 shows that irrelevant of the manikin height, the highest absolute f_p differences between a particular manikin and the average manikin occur in the 99% BMI cases (46 to 50 kgm⁻²) and can even reach 40% for the 1% height (145 cm) female manikin (all maximum differences occur for top-down irradiation). In other words, even when scaled by the effective radiation area, individuals with very large BMI are exposed to noticeably more solar radiation at shallow zenith angles.

To provide further insight into the impact of BMI on f_p at low zenith angles, we created and simulated additional obese male and female manikins with 50% height (176 cm or 162 cm) and 80%, 85%, 90%, 95%, and 97.5% BMI (see plot in Fig. 3 for BMI values and the Supplemental Information for more details on these manikins). The plot in Fig. 3 shows that $f_p(\theta = 0^\circ)$ is nearly linearly dependent on the value of the BMI (in kgm⁻²) and that its rate of increase is about twice higher for the female (0.0013 per kgm⁻²) than for the male manikins (0.00076 per kgm⁻²). However, since the BMI percentiles for both genders are not normally distributed around the mean value, the rate of $f_p(\theta = 0^\circ)$ increase per percentile is not linear and is much higher for individuals with BMI above 80% (see

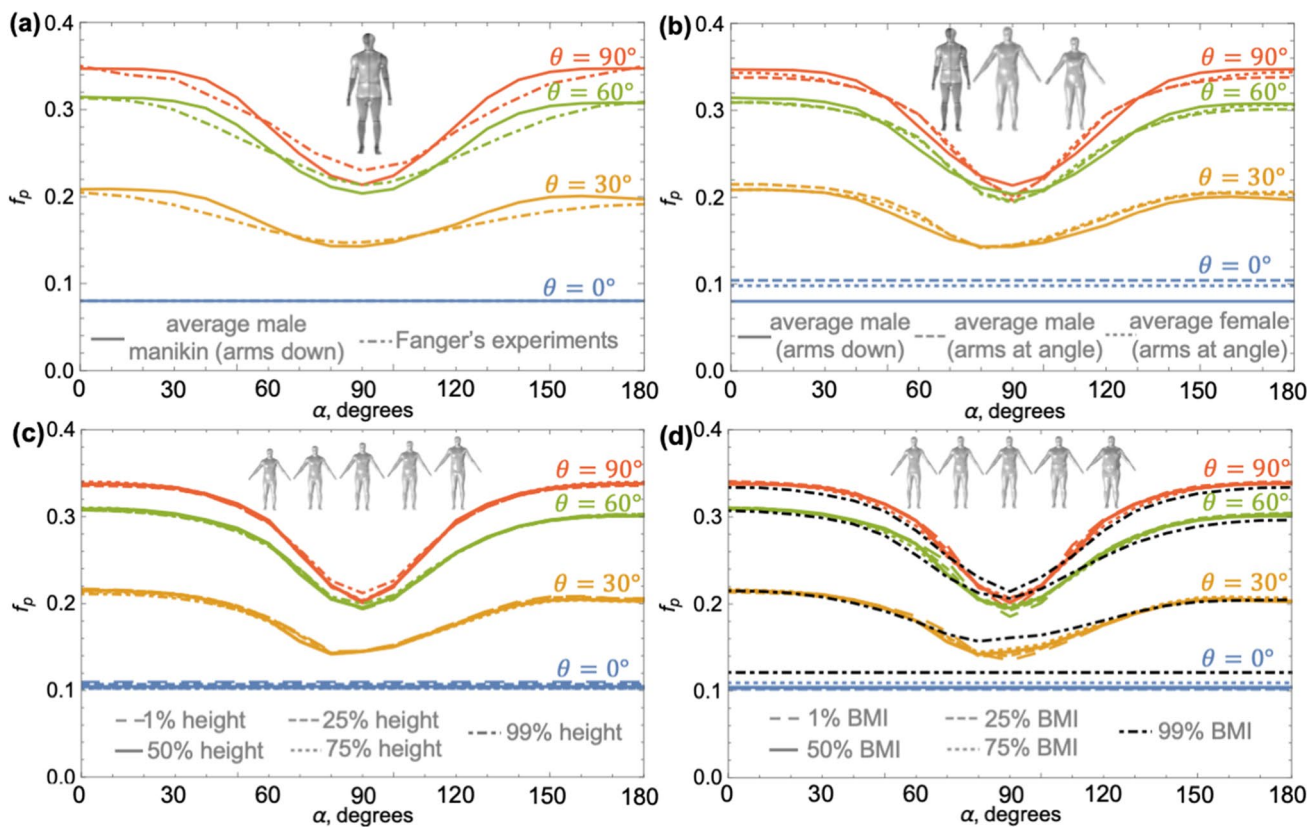


Fig. 2 The projected area radiation factor (f_p) distributions as a function of the azimuth angle (α) for four values of the zenith angle (θ) comparing **a** the simulated average (i.e., 50% BMI (28 kgm^{-2}) and 50% height (176 cm)) male manikin with arms down against Fanger’s experiments (Fanger 1972), **b** the simulated average male manikin with arms down and arms at an angle as well as the average female

manikin with the latter pose, **c** male manikins with 50% BMI (28 kgm^{-2}) and varying height percentile (1%-158 cm, 25%-171 cm, 50%-176 cm, 75%-181 cm, and 99%-195 cm), and **d** male manikins with 50% height (176 cm) and varied BMI ($1\text{-}18 \text{ kgm}^{-2}$, $25\text{-}25 \text{ kgm}^{-2}$, $50\text{-}28 \text{ kgm}^{-2}$, $75\text{-}32 \text{ kgm}^{-2}$, and $99\text{-}46 \text{ kgm}^{-2}$)

Table 2 The absolute maximum difference (in percent) in-between $f_p(\alpha, \theta)$ for the indicated and the average female or male manikins. All absolute maximum difference values occur for θ of 0° (i.e., top-down irradiation)

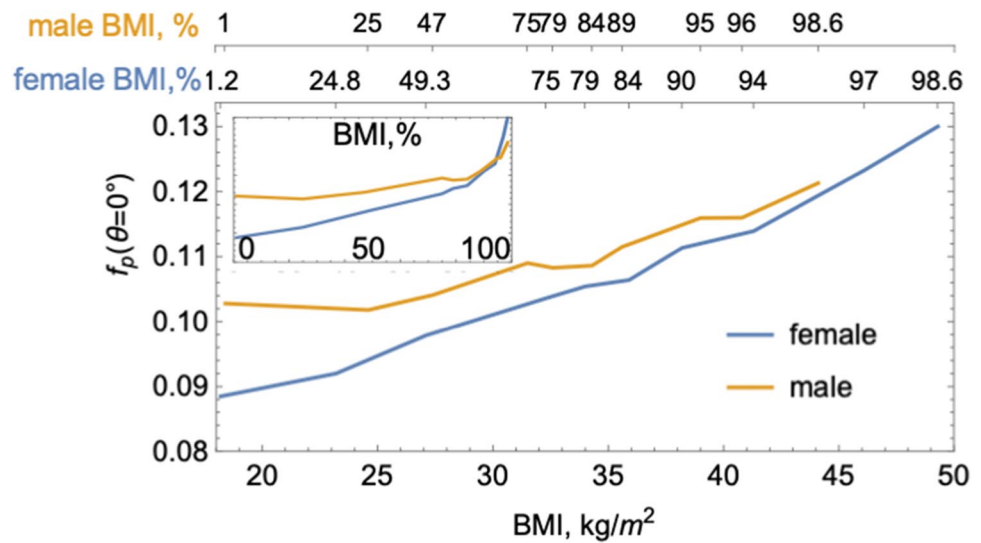
| BMI, % | Female manikin height, % | | | | | Male manikin height, % | | | | |
|--------|--------------------------|------|------|------|------|------------------------|------|------|------|------|
| | 1 | 25 | 50 | 75 | 99 | 1 | 25 | 50 | 75 | 99 |
| 1 | 3.5 | 13.6 | 9.6 | 11.2 | 14.1 | 6.6 | 7.5 | 8.6 | 6.7 | 7.9 |
| 25 | 2.2 | 5.3 | 6.2 | 8.4 | 10.9 | 4.8 | 1.7 | 3.9 | 3.2 | 6.2 |
| 50 | 11.3 | 2.4 | 0.0 | 5.7 | 7.8 | 5.8 | 4.3 | 0.0 | 2.8 | 5.2 |
| 75 | 9.7 | 4.8 | 5.8 | 3.7 | 7.8 | 8.4 | 5.8 | 4.9 | 3.6 | 7.8 |
| 99 | 42.0 | 31.1 | 32.9 | 34.6 | 23.9 | 26.9 | 19.9 | 17.0 | 23.0 | 14.3 |

inset plot in Fig. 3). We iterate that BMI only affects the f_p at shallow zenith angles and has comparable impacts to minor pose changes (e.g., arm position). In addition, the 0.01 to 0.03 variation in the $f_p(\theta = 0^\circ)$ with these parameters is minute compared to the 0.1 to 0.25 changes in the f_p induced by zenith angle increase. To put these variations into further context, we discuss several geometrical simplifications of the human body in the next section.

Discussion

Our results demonstrated that the projected radiation area factor distributions match closely for most of our manikins and are only slightly different at shallow zenith angles for individuals with very large BMI percentile. To provide another perspective on these results, we use our comprehensive “anatomical” manikin set to quantify

Fig. 3 The projected area radiation factor for top-down irradiation ($f_p(\theta = 0^\circ)$) for female and male manikins with 50% height (162 cm for female or 176 cm for male) and varied BMI values (the inset shows the same plot against the population BMI percentile). The percentiles corresponding to the BMI values for the male and female manikins are included on the two top horizontal axes

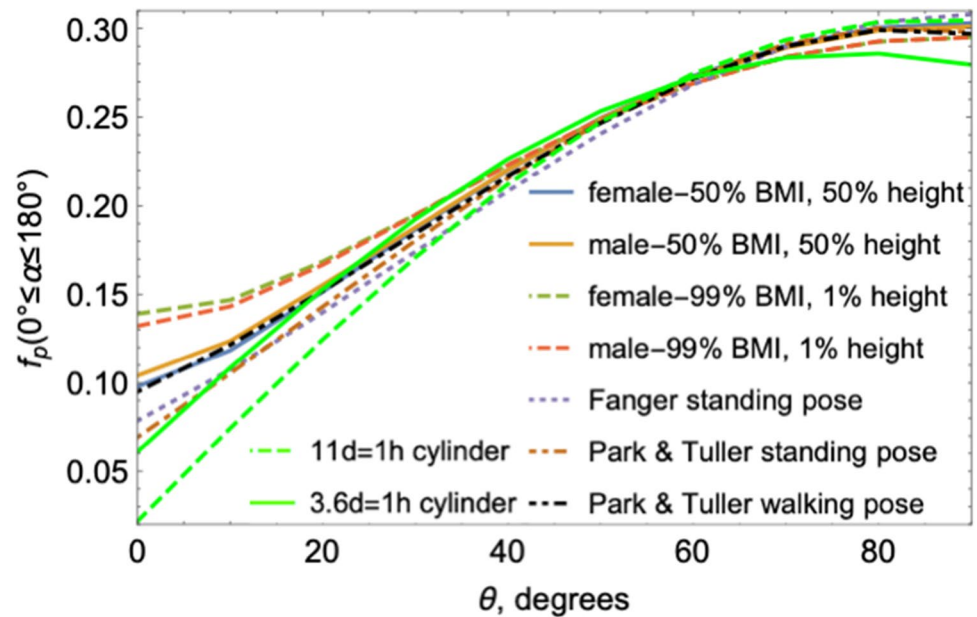


how modeling the human-environmental radiation heat exchange is impacted by several levels of the human body geometrical simplification. We examine the box or “peg” human (Höppe 1992; Holmer et al. 2015), the rotationally symmetric standing human (Staiger and Matzarakis 2020), and sphere and multi-cylinder human (Fiala et al. 1999; Fiala and Havenith 2015; Xu et al. 2019) body representations. The box or “peg” (Holmer et al. 2015; Brown 2019) representation of the human body is commonly used in the context of the integral radiation measurement (IRM) technique (Höppe 1992; Thorsson et al. 2007; Middel and Krayenhoff 2019; Vanos et al. 2021) to convert short and long wave irradiation fluxes originating from six directions (cardinal, top, and bottom) into effective irradiation flux experienced by an individual. The conversion is obtained by weighting the measurements in the cardinal directions (that are all parallel to the ground) with a 0.22 shape factor and those in the perpendicular directions (i.e., top and bottom) with a $(1-4 \times 0.22)/2 = 0.06$ shape factor. Höppe obtained the 0.22 shape factor by averaging the f_p distribution measured by Fanger (1972) across the entire range of zenith and azimuth angles (Höppe 1992). Remarkably, when we followed the same procedure, we found that all our manikins have an average f_p that rounds off to 0.22 and is at most 0.226 in the 99% BMI (50 kg m^{-2}) and 1% height (145 cm) female model case (see the Supplemental Information). This value is independent of the manikins’ body shape because, even at extreme values of BMI, the f_p is impacted only at shallow zenith angles. These parameters become more apparent when the complexity of the human body’s geometrical representation is increased by one level.

Representing the human body as rotationally symmetric is a practical way to incorporate the f_p distributions into human thermophysiological models and indices calculations (Jendritzky et al. 1990; Park and Tuller 2011a, b; Staiger and

Matzarakis 2020) and design simple radiation thermometers such as globes (Vernon 1932; de Dear 1988; Thorsson et al. 2007) and cylinders (Brown and Gillespie 1986; Krysz and Brown 1990; Brown 2019; Vanos et al. 2021). The plot in Fig. 4 shows distributions of projected radiation area factors averaged across all azimuth angle values for each simulated zenith angle value ($f_p(0^\circ \leq \alpha \leq 180^\circ)$) for our average and most “diverging” manikins (i.e., 99% BMI and 1% height). The plots also show fit to Fanger’s data used in Klima-Michel-Modell (Jendritzky et al. 1990; Staiger and Matzarakis 2020) and fits to Park and Tuller’s (2011a) results for standing and walking postures (these empirical formulas are presented in the Supplemental Information). All these $f_p(0^\circ \leq \alpha \leq 180^\circ)$ distributions essentially overlap for θ above 30° and below this angle diverge into groups based on the BMI and the pose. The male and female manikins with the 99% BMI and 1% height (and arms raised away from the trunk) have the highest $f_p(0^\circ \leq \alpha \leq 180^\circ)$ with 0.13 to 0.14 at $\theta = 0^\circ$. This value drops to about 0.1 for the next group of distributions that includes both our average male and female manikins with arms raised away from the trunk and Park and Tuller’s fit for walking posture (Park and Tuller 2011a). We attribute the agreement between these three distributions to close match of the degree to which arms are swung away from the body during walking and, albeit in different direction, are raised away from our manikins in the standing pose. In addition, as we discussed in the “Introduction” section, Park and Tuller’s (2011a) study covered subjects with BMI near the current average value for the USA (Center for Disease Control and Prevention 2022). The next group that includes the two fits for the standing pose with arms along the trunk has the lowest $f_p(0^\circ \leq \alpha \leq 180^\circ)$ distributions with the 0.08 at $\theta = 0^\circ$ expected from Fanger’s experiments (Fanger 1972). Lastly, the two green curves in Fig. 4 show $f_p(\theta)$ distributions for cylinders with a 3.6:1 and a 11:1 diameter-to-height ratio (Rykcaczeński et al. 2022). The shorter cylinder has an aspect ratio

Fig. 4 The rotationally symmetric humans: the projected area radiation factor averages across the azimuth angle range ($f_p(0^\circ \leq \alpha \leq 180^\circ)$) as a function of the zenith angle for the simulated 50% BMI (27 kgm^{-2} for male or 28 kgm^{-2} for female) and 50% height (176 cm for male and 162 cm for female) and 99% BMI (46 kgm^{-2} for male or 50 kgm^{-2} for female) and 1% height (158 cm for male and 145 cm for female) manikins, fit to Fanger's experiments (Fanger 1972; Staiger and Matzarakis 2020), Park and Tuller's standing and walking pose fits (Park and Tuller 2011a), and cylinders with diameter-to-height aspect ratios of 11:1 and 3.6:1



corresponding to IRM shape weighting factors (Holmer et al. 2015). The taller cylinder has an aspect ratio used for cylindrical radiation thermometers (Brown and Gillespie 1986; Krysz and Brown 1990; Brown 2019; Vanos et al. 2021). Considering their simplicity, both cylinders provide a surprisingly good match for a rotational human for most of the zenith angle range. The taller cylinder only underestimates values for θ below about 3° while the short cylinder only underestimates values for θ above about 7° . Next, we discuss whether multiple cylinders and a sphere can capture the f_p for the entire zenith and azimuth angle range for diverse human body shapes.

We developed three “tin-man” manikins to quantify to what degree the radiative area factors are impacted by the simplification of the human body to a set of cylinders and spheres (Fiala et al. 1999; Fiala and Havenith 2015; Xu et al. 2019). Specifically, we generated three male “tin-man” manikins with height and total surface area matching those of the anatomically representative manikins with 50% height (175 cm) and 1% (18 kgm^{-2}), 50% (28 kgm^{-2}), and 99% (46 kgm^{-2}) BMI. We based the 50% BMI manikin on Fiala's original model (Fiala et al. 1999) but empirically adjusted the lengths of the segments to provide a better match to our anatomically representative manikin. As shown in Fig. 5a, we subsequently scaled this “average” tin-man to fit the other two anatomical manikins. Demonstrating the close match between corresponding tin-man and anatomical manikins, the total and radiative surface areas of the two human body types are within a few square centimeters (see Table 3). Furthermore, the plots in Fig. 5b–d demonstrate that from the radiation perspective, the tin-mans are an acceptable representation of the anatomical manikins, with minor differences mainly emerging for shallow zenith angles and the largest BMI percentile.

Conclusions

Motivated by the lack of radiative area factors for half of the population of the USA with above-average BMI, we developed sixty anatomical computational manikins representing the 1 to 99% BMI and height diversity of the adults in the country. Our simulations revealed that the effective and projected radiation area factors angular distributions are nearly independent of gender, height, and BMI. Appreciable relative differences from the distributions for the average models (50% BMI and 50% height) only emerged for computational manikins with BMI above about 80% (33 to 34 kgm^{-2}) and are comparable to changes induced by pose change (e.g., raising arms away from the trunk). However, these differences only occur at shallow zenith angles (below 20°) and are small as compared to variations induced by zenith angle increase (i.e., $\Delta f_p / \Delta \theta \gg \Delta f_p / \Delta \text{BMI}$). The limited impact of the body shape on the radiative factors is highlighted by the average f_p for the entire angular distribution rounding off to 0.22 for all the computational manikins. For field radiation measurements, this implies that the shape factors employed in the IRM technique are representative of the entire adult population. In contrast, the BMI influence was apparent when the f_p was averaged only across the azimuth angle range. In particular, the resulting $f_p(0^\circ \leq \alpha \leq 180^\circ)$ distributions for the rotationally symmetric humans were, as expected, impacted by the highest value of BMI but only for zenith angles lower than 20° . Thus, once scaled by the surface area, the human body shape nearly has no impact on radiative heat transfer within the scope of the effective radiation factor approach.

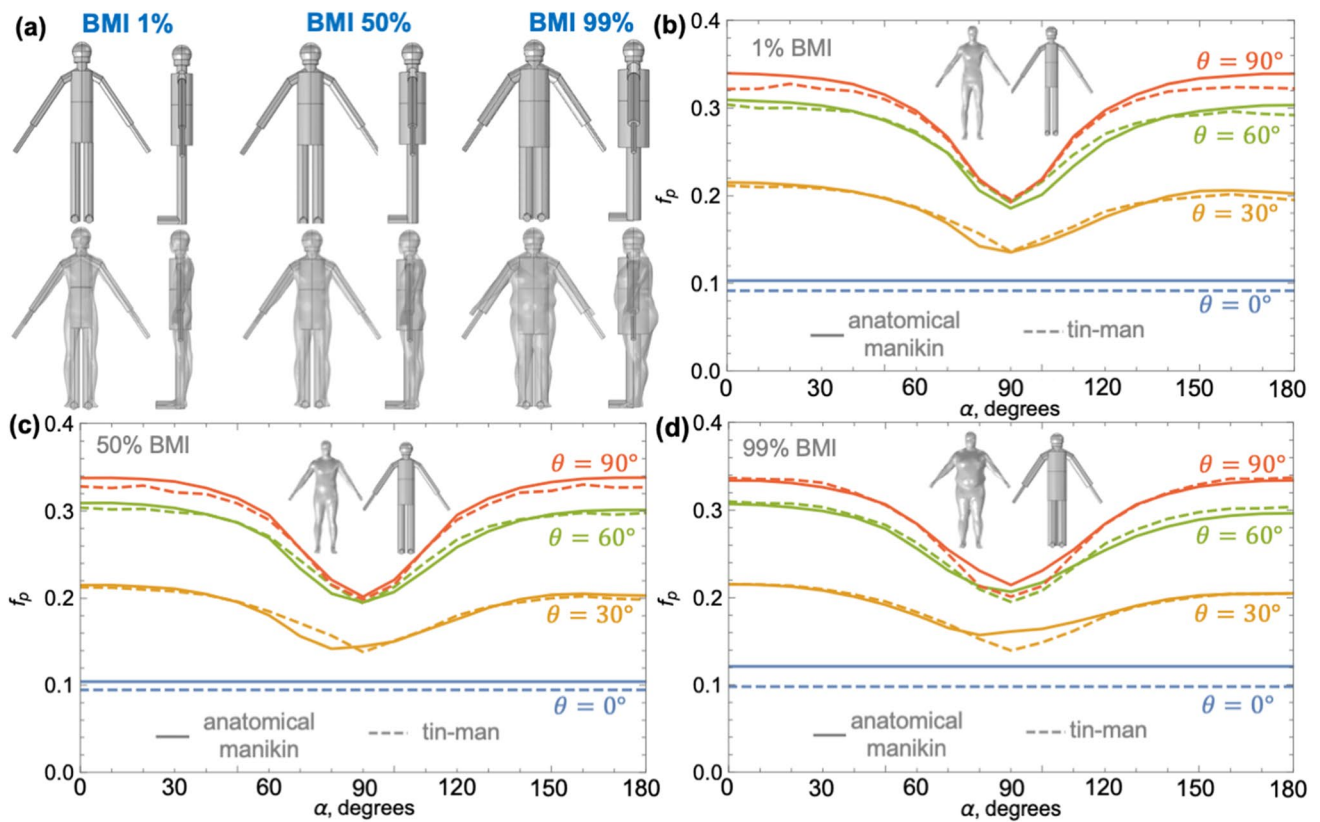


Fig. 5 a Front and side views of additional three tin-man manikins and their overlay with the corresponding anatomical male manikins with 50% height (175 cm) and 1% (18 kgm⁻²), 50% (28 kgm⁻²), and

99% (46 kgm⁻²) BMI; the f_p distributions for the **b** 1% (18 kgm⁻²) BMI, **c** 50% (28 kgm⁻²) BMI, and **d** 99% (46 kgm⁻²) BMI anatomical and tin-man manikins

Table 3 Total surface areas, effective radiation areas, and effective radiation area factors for average male manikin anatomical and simplified hands.

| Geometry | BMI 1%, H 50% | | BMI 50%, H 50% | | BMI 99%, H 50% | |
|------------------------------------|--------------------|---------|--------------------|---------|--------------------|---------|
| | Anatomical manikin | Tin man | Anatomical manikin | Tin man | Anatomical manikin | Tin man |
| H (cm) | 177 | 177.5 | 176 | 178 | 176 | 177.4 |
| A _{tot} (m ²) | 1.58 | 1.60 | 1.89 | 1.88 | 2.22 | 2.23 |
| A _{eff} (m ²) | 1.46 | 1.41 | 1.73 | 1.65 | 2.03 | 1.92 |
| f _{eff} | 0.92 | 0.88 | 0.92 | 0.88 | 0.92 | 0.87 |

While the effective radiation factor approach only provides information on the total body radiation exposure, the comprehensive set of anatomical manikins or their multi-cylinder and sphere avatars can be used to compute how body shape impacts a variety of external heat transport processes. For example, with minor adjustments (i.e., mitten-finger hand shape to capture given phenomena), the manikins can be employed to quantify body shape’s impact on the total and local convective heat transfer coefficients. The manikins can also be employed to simulate detailed heat exposure maps across the body in various scenarios. Such detailed heat flux body mapping can provide insight into thermal exposure in highly anisotropic conditions (Fiala et al. 1999; Rees et al.

2008; Zani et al. 2019; Aviv et al. 2020, 2022) and potentially be used to optimize localized thermal management systems (Vesely and Zeiler 2014; Rawal et al. 2020; Yang et al. 2021) for the broad population.

Supplementary Information The online version contains supplementary material available at <https://doi.org/10.1007/s00484-022-02362-7>.

Acknowledgements The authors would like to acknowledge Dr. Jason Yalim and Rebecca Belshe from the Research Computing Core Facilities at Arizona State University (ASU) for their aid with the simulation implementation on the ASU supercomputer. The authors also acknowledge Research Computing at ASU for providing High Performance Computing resources that have contributed to the research results

reported within this paper and partially support from the ASU Fulton Schools of Engineering 2021–2022 seed funding.

Author contribution Conceptualization: KR. Methodology: KR, LB, DMM, SHV. Analysis: KR, LB, DMM, SHV. Writing – original draft: KR. Writing – review and editing: KR, LB, DMM, SHV. Final review and editing: KR, LB, DMM, SHV.

Funding Arizona State University Fulton Schools of Engineering 2021–2022 Strategic Interest Seed Funding Program.

Data availability The manikin models are available on the ASU Dataverse website (<https://doi.org/10.48349/ASU/ZCLKT6>).

Declarations

Conflict of interest The authors declare no competing interests.

References

- Aviv D, Gros J, Alsaad H et al (2022) A data-driven ray tracing simulation for mean radiant temperature and spatial variations in the indoor radiant field with experimental validation. *Energy Build* 254:111585
- Aviv D, Hou M, Teitelbaum E et al (2020) Simulating invisible light: adapting lighting and geometry models for radiant heat transfer. In: *Proceedings of Symposia Simulation Architectural Urban Design* pp 311–318
- Bandow F, Bohnenkamp H (1935) Über die Bestimmung der Strahlungsfläche des Menschen aus seiner elektrischen Kapazität. *Pflüger's Archiv Für Die Gesamte Physiologie Des Menschen Und Der Tiere* 236:427–434
- Blazejczyk K, Nilsson H, Holmér I (1993) Solar heat load on man. *Int J Biometeorol* 37:125–132
- Brown RD (2019) Correcting the error in measuring radiation received by a person: introducing cylindrical radiometers. *Sensors* 19:5085
- Brown RD, Gillespie TJ (1986) Estimating outdoor thermal comfort using a cylindrical radiation thermometer and an energy budget model. *Int J Biometeorol* 30:43–52
- Center for Disease Control and Prevention (2022) Adult obesity facts. <https://www.cdc.gov/obesity/data/adult.html>. Accessed 13 Mar 2022
- de Dear R (1988) Ping-pong globe thermometers for mean radiant temperatures. *H V Eng* 60:10–11
- de Dear RJ, Arens E, Hui Z, Oguro M (1997) Convective and radiative heat transfer coefficients for individual human body segments. *Int J Biometeorol* 40:141–156
- Dreyfuss H, Dreyfuss H (1967) *The measure of man: human factors in design*. 2nd Edition, Whitney library of design, New York
- Fanger PO (1972) *Thermal comfort*. McGraw-Hill Book Company, New York
- Fiala D, Lomas KJ, Stohrer M (1999) A computer model of human thermoregulation for a wide range of environmental conditions: the passive system. *J Appl Physiol* 87(5):1957–1972
- Fiala D, Havenith G (2015) Modelling human heat transfer and temperature regulation. In: Gefen, Al, Epstei, Y. (eds) *The mechanobiology and mechanophysiology of military-related injuries*. Studies in mechanobiology, Tissue Engineering and Biomaterials, 19. Springer, Cham, pp 265–302
- Guibert A, Taylor CL (1952) Radiation area of the human body. *J Appl Physiol* 5:24–37
- Holmer B, Lindberg F, Rayner D, Thorsson S (2015) How to transform the standing man from a box to a cylinder—a modified methodology to calculate mean radiant temperature in field studies and models. In: *Proceedings of the 9th International Conference on Urban Climate (ICUC9)*, Toulouse, France. pp 20–24
- Höppe P (1992) Ein neues Verfahren zur Bestimmung der mittleren Strahlungstemperatur im Freien. *Wetter Und Leben* 44:147–151
- Horikoshi T (1990) The effective radiation area and angle factor between man and a rectangular plane near him. *ASHRAE Trans* 96:60–66
- Hsu A, Sheriff G, Chakraborty T, Manya D (2021) Disproportionate exposure to urban heat island intensity across major US cities. *Nat Commun* 12:1–11
- Ioannou LG, Tsoutsoubi L, Mantzios K et al (2021) The impacts of sun exposure on worker physiology and cognition: multi-country evidence and interventions. *Int J Environ Res Public Health* 18:7698
- Jendritzky G, Menz G, Schmidt-Kessen W, Schirmer H *Methode zur Raumb-Zogenen Bewertung der Thermischen Komponente im Bioklima des Menschen (Fortgeschriebenes Klima-Michel-Modell)*; Akademie für Raumforschung und Landesplanung: Hannover, Germany, 1990. ISBN 3888382076 80
- Jones BW, Hong S, McCullough EA (1998) Detailed projected area data for the human body. *ASHRAE Trans* 104:1327
- Krys SA, Brown RD (1990) Radiation absorbed by a vertical cylinder in complex outdoor environments under clear sky conditions. *Int J Biometeorol* 34:69–75
- Kubaha K, Fiala D, Toftum J, Taki AH (2004) Human projected area factors for detailed direct and diffuse solar radiation analysis. *Int J Biometeorol* 49:113–129
- Kubaha K, Fiala D, Lomas KJ (2003) Predicting human geometry-related factors for detailed radiation analysis in indoor spaces. *Proceedings of 8th Int. IBPSA Conf.*, Eindhoven, Netherlands, 681–688
- Lasisi T, Smallcombe J, Shriver MD et al (2020) Hair fiber morphology and function: at the intersection of anthropology, physiology, and engineering. *FASEB J* 34:1
- Manabe M, Yamazaki H, Sakai K (2004) Shape factor simulation for the thermal radiation environment of the human body and the VRML visualization. *Build Environ* 39:927–937
- Middel A, Krayenhoff ES (2019) Micrometeorological determinants of pedestrian thermal exposure during record-breaking heat in Tempe, Arizona: introducing the MaRTy observational platform. *Sci Total Environ* 687:137–151
- Mitchell D, Wyndham CH, Vermeulen AJ et al (1969) Radiant and convective heat transfer of nude men in dry air. *J Appl Physiol* 26:111–118
- Park S, Tuller SE (2011a) Human body area factors for radiation exchange analysis: standing and walking postures. *Int J Biometeorol* 55:695–709
- Park S, Tuller SE (2011b) Comparison of human radiation exchange models in outdoor areas. *Theor Appl Climatol* 105:357–370
- Parkinsons M (n.d.) Open Design Lab Manikin Fetcher. <http://tools.openlab.psu.edu/tools/fetcher.php>. Accessed 9/5/2022
- Parsons K (2014) *Human thermal environments: the effects of hot, moderate, and cold environments on human health, comfort, and performance*. CRC Press, New York
- Quintela D, Gaspar A, Borges C (2004) Analysis of sensible heat exchanges from a thermal manikin. *Eur J Appl Physiol* 92:663–668
- Rawal R, Schweiker M, Kazanci OB et al (2020) Personal comfort systems: a review on comfort, energy, and economics. *Energy Build* 214:109858
- Redlarski G, Palkowski A, Krawczuk M (2016) Body surface area formulae: an alarming ambiguity. *Sci Rep* 6:1–8
- Rees SJ, Lomas KJ, Fiala D (2008) Predicting local thermal discomfort adjacent to glazing. *ASHRAE Trans* 114:1–10

- Rizzo G, Franzitta G, Cannistraro G (1991) Algorithms for the calculation of the mean projected area factors of seated and standing persons. *Energy Build* 17:221–230
- Rykaczewski K, Vanos JK, Middel A (2022) Anisotropic radiation source models for computational thermal manikin simulations based on common radiation field measurements. *Build Environ* 208:108636
- Smallcombe JW, Hodder S, Kuklane K et al (2021) Updated database of clothing thermal insulation and vapor permeability values of western ensembles for use in ASHRAE standard 55, ISO 7730, and ISO 9920. *ASHRAE Trans* 127:773–800
- Staiger H, Matzarakis A (2020) Accuracy of mean radiant temperature derived from active and passive radiometry. *Atmosphere (basel)* 11:805
- Steinman M, Kalisperis LN, Summers LH (1988) Angle factor determination from a person to inclined surfaces. *ASHRAE Trans* 94:1809–1823
- Tanabe S, Narita C, Ozeki Y, Konishi M (2000) Effective radiation area of human body calculated by a numerical simulation. *Energy Build* 32:205–215
- Thorsson S, Lindberg F, Eliasson I, Holmer B (2007) Different methods for estimating the mean radiant temperature in an outdoor urban setting. *Int J Climatol* 27:1983–1993
- Underwood CR, Ward EJ (1966) The solar radiation area of man. *Ergonomics* 9:155–168
- Vanos JK, Rykaczewski K, Middel A et al (2021) Improved methods for estimating mean radiant temperature in hot and sunny outdoor settings. *Int J Biometeorol* 65:967–983
- Vernon HM (1932) The measurement of radiant heat in relation to human comfort. *J Ind Hyg* 14:95–111
- Vesely M, Zeiler W (2014) Personalized conditioning and its impact on thermal comfort and energy performance—a review. *Renew Sustain Energy Rev* 34:401–408
- Winslow C-E, Gagge AP, Herrington LP (1940) Heat exchange and regulation in radiant environments above and below air temperature. *Am J Physiol-Legacy Content* 131:79–92
- Wissler EH (2018) *Human temperature control: a quantitative approach*, 1st edn. Springer, Berlin, Germany
- Xu J, Psikuta A, Li J et al (2019) Influence of human body geometry, posture and the surrounding environment on body heat loss based on a validated numerical model. *Build Environ* 166:106340
- Yang B, Ding X, Wang F, Li A (2021) A review of intensified conditioning of personal micro-environments: moving closer to the human body. *Energy Built Environ* 2:260–270
- Yousaf R, Fiala D, Wagner A (2008) Numerical simulation of human radiation heat transfer using a mathematical model of human physiology and computational fluid dynamics (CFD). In: Nagel, W.E., Kroner, D., Resch, M. (eds) *High performance computing in science and engineering'07*. Springer, Berlin, pp 647–666
- Zani A, Richardson HD, Tono A et al (2019) A simulation-based design analysis for the assessment of indoor comfort under the effect of solar radiation, *Proceeding of symposium on simulation for architecture and urban design*, Georgia Tech, Atlanta, USA
- Springer Nature or its licensor holds exclusive rights to this article under a publishing agreement with the author(s) or other rightsholder(s); author self-archiving of the accepted manuscript version of this article is solely governed by the terms of such publishing agreement and applicable law.